Monoliths as Suitable Catalysts for Reverse-Flow Combustors: Modeling and Experimental Validation

Pablo Marín, Salvador Ordóñez, and Fernando V. Díez
Dept. of Chemical Engineering and Environmental Technology, Facultad de Química, University of Oviedo, Julián Clavería 8, Oviedo 33006, Spain

DOI 10.1002/aic.12215
Published online March 22, 2010 in Wiley Online Library (wileyonlinelibrary.com).

The performance of a bench-scale monolithic reverse-flow reactor (RFR) for methane combustion has been experimentally studied in this work. The influence of the different operating parameters, such as total gas flow rate (2.5×10^{-4}–5×10^{-4} m^3 s^{-1} (STP)), methane inlet concentration (1000–5500 ppm), and switching time (300–900 s) on the reactor performance (outlet conversion and stability), has been experimentally determined. The validation of a heterogeneous one-dimensional dynamic model for monolithic beds with the obtained experimental data allows the use of this model to simulate the behavior of industrial-scale reactors. In the second part of the work, a systematic comparison of particulate and monolithic RFRs is carried out through design curves. Reactor length for 99% outlet conversion and the corresponding pressure drop is determined for varying operating conditions (surface velocity and inlet methane concentration). © 2010 American Institute of Chemical Engineers *AIChE J,* 56: 3162–3173, 2010

Keywords: unsteady-state processes, lean hydrocarbon–air mixtures, structured catalyst, methane combustion, catalytic combustion

Introduction

The concern about methane emissions has drastically risen in the last years, because this gas is the second contributor to global warming after carbon dioxide. In fact, methane has a global warming potential 23 times higher than carbon dioxide, so there is a clear advantage into oxidizing the methane present in gaseous emissions to carbon dioxide, before releasing to the atmosphere.[1] Moreover, methane is also a very important model compound for catalytic combustion, because it is one of the hydrocarbons more difficult to treat.[2] As a result, a good performance of the reactor with methane can easily be extended to other hydrocarbons. In many situations, such as in mine ventings,[3] methane concentration is high enough to recover part the heat of reaction, generating hot water, steam, or even electricity, and thus improving the economy of the process.[4]

The reverse-flow reactor (RFR) is an alternative treatment for gaseous emissions containing hydrocarbons, based on the catalytic combustion. Its main advantage is the high thermal efficiency, which allows the autothermal operation (with low temperature feeding and without auxiliary fuel), even for emissions with very low hydrocarbon concentration (20–30°C of adiabatic temperature rise).[5] This technique also allows the treatment at low pressures, contrary to other innovative combustion techniques such as catalytic gas turbines or superadiabatic lean catalytic combustion.[6] The RFR operates under forced unsteady-state conditions, created by periodically reversing the feed flow direction. Therefore, the heat released during the exothermic reaction is trapped inside the reactor bed between two consecutive flow reversals, being used to preheat the cold feed up to the reaction temperature. As a result, the RFR is an integrated device where both reaction and heat exchange take place with high

Correspondence concerning this article should be addressed to S. Ordóñez at sordonez@uniovi.es.

thermal efficiency. Further explanations about this technology and its applications are exhaustively reported in recent reviews and articles cited therein.[7–9]

Catalytic combustion of hydrocarbons in RFR using particulate catalysts (spheres, extrudates, Raschig rings, etc) has been extensively studied by different authors.[5,10,11] However, if the RFR technology is extended to real emissions, the particulated beds must be replaced by monoliths, which are the devices able to manage high flow rates with affordable pressure drops.[9,12] This work is motivated by the few experimental studies about monolithic RFR appearing in the literature: Nieken and Eigenberger[13,14] studied the combustion of propane and propylene using Pd and Pt monoliths, Ramdani et al.[15] considered the combustion of xylene at low switching times and tested a control system, Litto et al.[16] studied the combustion of methane, but using rings as catalyst and monoliths only as inert beds, and more recently Gosiewski et al.[17] compared the performance of inert pellets and monoliths for the homogeneous (noncatalytic) combustion of methane. This work tries to fill this gap performing a detailed experimental study for methane combustion in a bench-scale RFR, where both inert and catalytic sections are filled with monolith beds.

The main problem for extending the RFR technology to monolithic beds is the lower thermal inertia compared to particulate beds, which makes the reactor more unstable.[18] However, this fact can be overcome by oversizing the reactor dimension or changing operation conditions (switching time, adding external fuel, etc.). For doing this, a systematic and experimentally validated comparison of both bed types is required for the RFR. In this work, this is accomplished by computer simulations of the RFR performance, using an experimentally validated model.

Experimental Device

Methane catalytic combustion has been studied in a bench-scale RFR. The reactor, a 0.8 m length, 0.05 m internal diameter, 316 stainless steel tube, houses the monolithic beds. The catalytic monolith (0.250 m length) is situated in the middle, whereas two inert cordierite beds (0.125 m length each) are situated at both sides. The beds are surrounded by a glass wool layer to avoid gas bypasses near the reactor wall. The temperature of the bed is measured in 7 points along the reactor axis. The absence of radial temperature profiles has been checked using a test thermocouple. The unit is equipped with a temperature control system, which avoids the heat losses through the reactor wall. This unit, designed specifically for the RFR, in which temperature varies with both time and reactor length, has been described in detail in the previous works.[10] This configuration allows working under near-adiabatic conditions, as industrial reactors with larger diameters. Moreover, as the wall heat transfer coefficient and radial thermal conductivity of monolithic beds are lower than the corresponding to particulate beds,[9] the influence of the stainless steel wall on the thermal behavior of the reactor, reported by Hevia et al.[19] for packed-beds, is considered negligible for monolithic beds.

The flow reversal is accomplished by using two pairs of solenoid valves (Parker-Lucifer 121K46E), acting on the reactor inlet and outlet streams. Reactor feed, consisting of methane–air mixture with different methane concentrations, is set using two mass flowmeters (Bronkhorst F201C). The analysis of methane concentration at the inlet and outlet streams is performed continuously (each 5 s) using an infrared spectrometer (ABB- PIR3502). With this analytical procedure, it is possible to measure the washout phenomena caused by the punctual emission of the methane contained in the inert beds when the feed flow is reversed.

Table 1. Physical and Geometrical Properties of the Inert and Catalyst Beds Used in the Monolithic Reverse-Flow Reactor

	Catalyst	Inert
Material	Pd/CeO_2-ZrO_2/cordierite	Cordierite
Hydraulic diameter, D_h (m)	0.97×10^{-3}	1.4×10^{-3}
Cell density (cells/m^2) (cpsi)	5.72×10^5 (370)	3.09×10^5 (200)
Bed porosity, ε	0.54	0.60
Density, ρ (kg m^{-3})	1900	2100
Heat capacity, C_p (J kg^{-1} K^{-1})	900	900
Thermal conductivity, κ (W m^{-1} K^{-1})	0.8	1

The selection of a suitable catalyst to carry out the combustion of methane is of great importance for the operation of the RFR. Thus, methane catalytic oxidation exhibits low reaction rate, in comparison to other hydrocarbons, requiring catalysts with high stability at high temperatures. In the previous works, working with particulate fixed-bed reactors, we have observed that it is difficult to get stable operation working with not very active catalysts, such as metal oxides.[20] It is widely accepted that Pd-based noble metal catalysts are the most active for methane combustion,[2] but it is also well known that the most common supports, such as alumina or silica, can present thermal deactivation at the reaction temperatures. As a result, alternative supports were proposed, being zirconia-based ones the most promising because of their high thermal stability.[21] In this context, a commercial Pd/CeO_2-ZrO_2/cordierite monolith supplied by Engelhard (REX-1708) has been used in this work. The geometric and physical properties of the catalyst and inert material are summarized in Table 1.

Mathematical Modeling of Monolithic RFR

The modeling of the dynamic reactor is essential for the systematic study of the reactor performance, comparison of different reactor configurations, scale-up purposes, etc.[18,19,22,23] As the modeling of these systems requires the estimation of many physical properties, kinetic and transport parameters, the experimental validation of the model is necessary to ensure the accuracy of subsequent simulations.

In this work, only one single channel of the monolith bed is simulated, assuming all the others have exactly the same behavior.[9] The reactor is considered to work under adiabatic conditions (no heat transfer from the reactor wall to the surrounding is taken into account), as will be experimentally demonstrated. The following heterogeneous 1D dynamic model has been obtained from conservation equations applied separately to the gas and solid phases:

Mass balance to the gas phase:

$$\frac{\partial y_{Gj}}{\partial t} = -\frac{u_0}{\varepsilon}\frac{\rho_{G0}}{\rho_G}\frac{\partial y_{Gj}}{\partial z} + D_{ax}\frac{\partial^2 y_{Gj}}{\partial z^2} - a_G K_{Gj}(y_{Gj} - y_{Sj}). \quad (1)$$

Mass balance to the solid phase:

$$\frac{\partial y_{Sj}}{\partial t} = a_S K_{Gj}(y_{Gj} - y_{Sj}) + \frac{\eta_j \rho_{cat}(r_j)_m}{C_G}. \quad (2)$$

Energy balance to the gas phase:

$$\frac{\partial T_G}{\partial t} = -\frac{u_0}{\varepsilon}\frac{\rho_{G0}}{\rho_G}\frac{\rho T_G}{\rho z} + \frac{k_{G,ax}}{\rho_G C_{pG}}\frac{\partial^2 T_G}{\partial z^2} + \frac{a_G h}{\rho_G C_{pG}}(T_S - T_G). \quad (3)$$

Energy balance to the solid phase:

$$\frac{\partial T_S}{\partial t} = \frac{k_S}{\rho_S C_{pS}}\frac{\partial^2 T_S}{\partial z^2} + \frac{a_S h}{\rho_S C_{pS}}(T_G - T_S) + \frac{\sum_{j=1}^{C}\eta_j \rho_{cat}(r_j)_m \Delta H_j}{\rho_S C_{pS}}. \quad (4)$$

Mechanical energy balance:

$$\frac{\partial p}{\partial z} = -\frac{2f_F(\rho_{G0}u_0)^2}{D_h \rho_G}, \quad p|_{z=0} = p_0. \quad (5)$$

Initial conditions:

$$y_G|_{t=0} = y_S|_{t=0} = 0, \quad T_G|_{t=0} = T_S|_{t=0} = T_{ph}. \quad (6)$$

Boundary conditions (Danckwerts boundary conditions):

$$(y_{Gj})_{0^-} = (y_{Gj})_{0^+} - \frac{\varepsilon D_{ax}}{u_0}\left(\frac{\partial y_{Gj}}{\partial z}\right)_{0^+}, \quad (7)$$

$$(T_G)_{0^-} = (T_G)_{0^+} - \frac{\varepsilon k_{G,ax}}{u_0 \rho_{G0} C_{pG}}\left(\frac{\partial T_G}{\partial z}\right)_{0^+}, \quad (8)$$

$$\left(\frac{\partial y_{Sj}}{\partial z}\right)_{z=0^+} = \left(\frac{\partial T_S}{\partial z}\right)_{z=0^+} = 0, \quad (9)$$

$$\left(\frac{\partial y_{Gj}}{\partial z}\right)_{z=L_R} = \left(\frac{\partial y_{Sj}}{\partial z}\right)_{z=L_R} = \left(\frac{\partial T_G}{\partial z}\right)_{z=L_R} = \left(\frac{\partial T_S}{\partial z}\right)_{z=L_R} = 0. \quad (10)$$

Homogenous gas-phase reaction has been neglected, because the working temperature is not high enough.[24] Ideal gas behavior for the gas phase is assumed. Transport and dispersion parameters appearing in the previous equations are calculated using the adequate expression for monoliths beds obtained from the literature.

Gas–solid mass transfer has been calculated using an empirical expression proposed by Ullah and Waldram,[25] Eq. 11, determined from experiments performed under developing hydrodynamic regime and reacting conditions (the range of application corresponds to typical conditions found in exhaust gas cleaning applications). The heat transfer coefficient is obtained from the Chilton-Colburn's analogy using an equivalent expression.

$$Sh = \frac{D_h K_G}{D_{AB}} = 0.766\left[\left(\frac{D_h}{L_{cat}}\right)Re\ Sc\right]^{0.483}. \quad (11)$$

The axial dispersion coefficients for the gas phase are calculated using the expressions proposed by Hayes and Kolaczkowski for laminar flow.[24] Reaction rate and internal effectiveness factor are studied in the following section, devoted to the kinetic study.

Regarding mass transfer, the Chilton-Colburn's analogy between mass and heat transfer was considered (equivalence between Sherwood and Nusselt numbers, on one hand, and Schmidt and Prandtl numbers, on the other hand).

The previous set of partial differential algebraic equations defines the mathematical model, which has been solved using the so-called "method of lines." The calculations have been done using a code written in MATLAB. According to this code, the space derivatives are approximated using finite differences in a grid of 150 points, and then the resulting set of ordinary differential algebraic equations is solved using the MATLAB function ode15s for stiff problems. The accuracy of this method has been demonstrated in the previous works.[18–20]

Determination of the Kinetic Parameters

The reaction kinetics when working with methane–air lean mixtures is usually modeled using a power-law rate expression depending on methane concentration.[26,27] As oxygen is generally in great excess with respect to methane, oxygen concentration remains constant, being the reaction rate independent from this parameter. Arrhenius dependence of the kinetic constant has also been assumed.

$$(r_j)_m = -k_{mj}(p_j)^b, \quad \text{with: } k_{mj} = k^0_{mj}\exp\left(-\frac{E_{aj}}{RT}\right). \quad (12)$$

The kinetic parameters (preexponential factor, activation energy, and the exponent b) must be determined experimentally. In this work, a fixed-bed isothermal reactor (400 mm length, 9 mm diameter) working under controlled conditions has been used. The monolith catalyst was crushed and sieved to a particle size of 230–355 μm, so that internal and external transport resistances can be neglected, and the intrinsic kinetic parameters determined. This assumption was checked once the parameters were determined by the calculation of the Carberry number (at 500°C, $Ca = 10^{-4} < 0.05$) and the Wheeler-Weisz criteria (at 500°C $\eta\phi^2 = 4 \times 10^{-7} < 0.1$).[28] Isothermal conditions are ensured by the small catalyst loading (1.01 g) and the use of inert diluents.

Experiments have been performed for different methane inlet concentrations and reactor temperatures. The kinetic parameters that best fit all the experimental data have been determined by means of the following minimization algorithm (13). The results have been collected in Table 2. The value obtained for the activation energy, 98 kJ mol^{-1}, is within the values reported in the literature for the low temperature region of methane combustion: 96 kJ mol^{-1},[29] 77 kJ mol^{-1},[22] and 95–125 kJ mol^{-1}.[26]

Table 2. Kinetic Parameters and Catalyst Properties for Monolithic Catalyst Used in this Work

Catalyst Properties	
Preexponential factor, k_m^0 (mol kg^{-1} s^{-1} Pa^{-1})	27.97
Activation energy, E_a (kJ mol^{-1})	98.4
Exponent, b	1.50
$\sum_{i=1}^{N}\left\|X_i - (X_i)_{exp}\right\|$	0.240
Mean pore diameter, $\langle d_{pore}\rangle$ (m)	6.8×10^{-8}
Internal porosity, ε_{pore}	0.12
Tortosuity, τ_{pore}	2
Washcoating thickness, L_w (m)	9×10^{-5}

$$\min \sum_{i=1}^{N} |X_i - (X_i)\,\mathrm{exp}|$$
$$\text{s.t. } \frac{dy_i}{dM_{cat}} = \frac{(r_i)_m}{F_{tot}},\ y_i|_{M_{cat}=0} = y_{i,0},\ i = 1,\ldots N \qquad (13)$$
$$X_i = 1 - \frac{y_i|_{M_{cat}=M_{cat,tot}}}{y_{i,0}}.$$

As the kinetic parameters have been determined in the absence of transport limitations, they are independent of the catalyst shape. As a result, to model the reactor properly, accurate internal effectiveness factors must be used. For the case of monolithic reactors, reactant mass transfer inside the catalyst washcoat layer can be important, particularly for fast reactions, such as catalytic combustion reactions. In this work, the following expression, valid for mass transfer to a flat slab, is used to determine the internal effectiveness factor[24]:

$$\eta_j = \frac{\tanh \phi_j}{\phi_j}. \qquad (14)$$

For the calculation of the Thiele modulus (ϕ_j), Eq. 15, derived from the generalized expression for the case of a power-law kinetic equation,[30] has been used. The effective diffusion coefficient accounts for molecular and Knudsen diffusion, using the information of Table 2.

$$\phi_j = L_w \sqrt{\frac{(b+1)\rho_{cat} k_{mj} R T_S}{2 f_w D_{eff}} \left(\frac{p y_{S_j}}{R T_S}\right)^{b-1}}. \qquad (15)$$

Reverse-Flow Reactor Operation

The first set of experiments has been devoted to ensure that the experimental device follows an adiabatic behavior. This behavior is the most typical in industrial units (because of the large diameter of these units), but it is difficult to achieve at bench scale (lower diameter and hence higher surface/volume ratio). Our device tries to achieve this behavior using a temperature control system, as described in the Experimental device section. The first experiment with this device loaded with the monolith catalyst was done without reactants, feeding the reactor with preheated air (at around 400°C) and only in one direction. The temperature profile at the end of the preheating stage with and without the control system activated is presented in Figure 1. It is observed that the temperature of the bed decreases considerably from the inlet to the outlet of the reactor when the temperature control system is switch off, because of the losses of part of the heat to the surroundings. On the contrary, if the temperature control system is activated at the beginning of the preheating stage, the heat transfer through the reactor wall is avoided, allowing a near-adiabatic behavior inside the reactor tube. This is experimentally demonstrated by the flat temperature profile depicted in Figure 1.

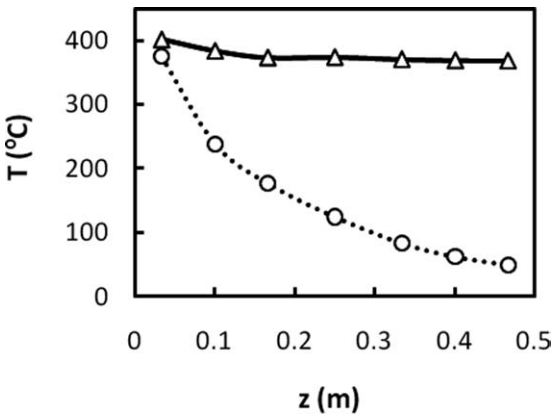

Figure 1. Temperature profile at the end of the preheating, with (Δ) and without (o) temperature control system.

$Q_{G0} = 1.83 \times 10^{-4}$ m^3 s^{-1} (STP).

Once the reactor adiabaticity has been experimentally proven, its behavior in a reactive environment has been checked. Figure 2 illustrates the evolution over a half-cycle of typical RFR temperature and conversion profile curves ($Q_{G0} = 2.5 \times 10^{-4}$ m^3 s^{-1} (STP), $y_{G0} = 1915$ ppm

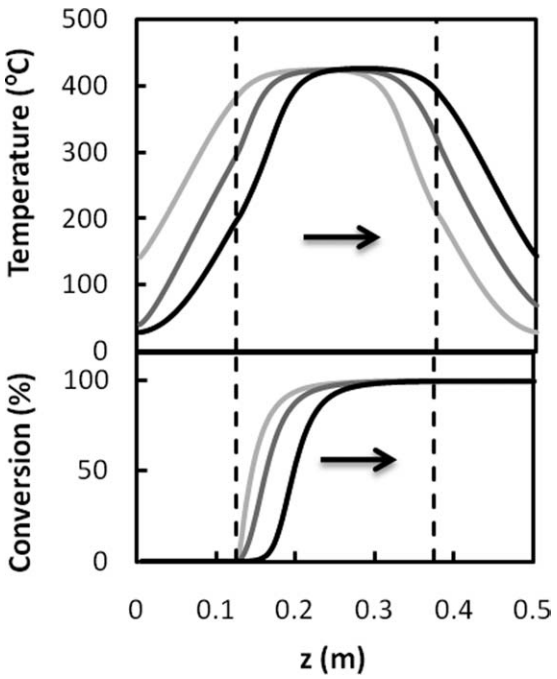

Figure 2. Typical temperature and conversion profiles of a reverse-flow reactor.

$Q_{G0} = 2.5 \times 10^{-4}$ m^3 s^{-1} (STP). $y_{G0} = 1915$ ppm methane. $t_{sw} = 300$ s. Flow direction is indicated by the arrow.

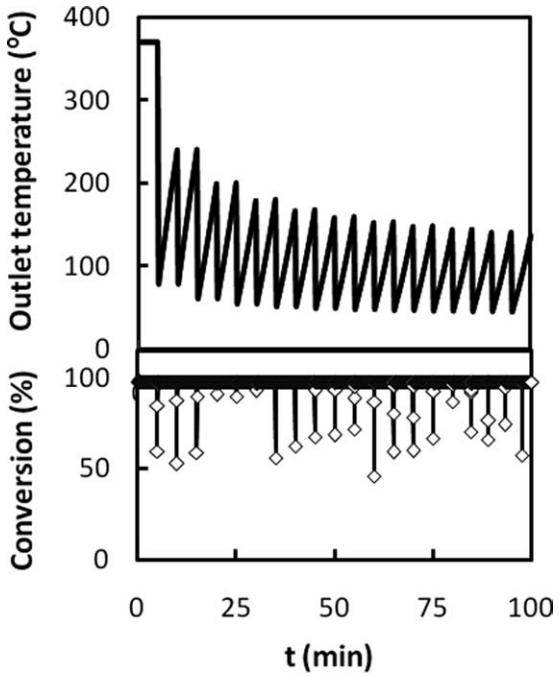

Figure 3. Evolution of the outlet gas temperature and conversion with the operation time.

$Q_{G0} = 2.5 \times 10^{-4}$ m^3 s^{-1} (STP). $y_{G0} = 1915$ ppm methane. $t_{sw} = 300$ s.

methane, $t_{sw} = 300$ s). After some cycles (in the so-called periodic pseudo-steady state), a characteristic high temperature plateau is formed in the middle of the bed. This profile is a consequence of the regenerative capacity of the reactor, when working with low temperature feeding (typically 25°C). Thus, the cold feed is preheated using the heat stored in the first inert bed, then the heat of reaction is released in the central catalytic bed, and finally part of the heat of the hot air exhaust stream is stored in the second inert bed before exiting the reactor. The temperature plateau moves in the direction of the flow as more cold air enters the reactor, so the flow direction must be reversed to avoid the extinction of the reactor. As the temperature at the reactor ends is too low for the reaction to take place, the catalyst is usually substituted in this region by an inert catalyst. In this work, half of the bed has been considered filled with catalyst, the other half with inert. Conversion profile curves exhibit a steady increase, which depends on the reaction rate and the reactor temperature.

The corresponding outlet temperature and conversion evolution with time are depicted in Figure 3. It is observed that the outlet temperature presents oscillations, which are repeated each half-cycle, as a consequence of the movement of the high temperature plateau. The outlet conversion has been calculated from the methane outlet and inlet concentrations, measured on line using an infrared spectrometer. Conversion presents repetitive and sudden decreases, which are caused by the emission of the unreacted methane of the inert beds and piping (between the reactor and the flow-reversal valves), when the switch of the flow direction is performed. This is usually known as the washout phenomena, which is inherent to the RFR technology.[20] However, the influence on the average outlet conversion is very low, particularly if operation with very low switching time values (lower than 20 s) is avoided.[31,32]

Influence of the Main Operating Conditions

Once it has been demonstrated that the experimental device performs properly, a more detailed study on the influence of the main operation condition on monolith RFR reactor has been carried out. The main operation conditions affecting the reactor behavior are total gas flow rate, methane feed concentration, and switching time. In this work, two total gas flow rates have been considered, 2.5×10^{-4} and 5×10^{-4} m^3 s^{-1} (STP), corresponding to linear velocities in the monolith bed of 0.31 and 0.61 m s^{-1} (measured at the inlet conditions, 25°C and 1.2 bar). Methane concentration has been varied from 940 to 6324 ppm (corresponding 26–175°C of adiabatic temperature rise). The switching time has been varied, depending of the methane concentration, from 100 to 900 s. Table 3 summarizes the values of these parameters for the experiments reported in this section. The influence of these variables on reactor performance can be analyzed following the experimental temperature profiles measured at the end of a half-cycle (the gas flowing from left to right), as depicted in Figure 4.

The effect of the total gas flow rate (Figure 4a), for constant methane inlet concentration and switching time, shows that the high temperature plateau moves through the bed at a higher velocity as the gas flow rate increases (keeping constant switching time and concentration). This effect causes a decrease of the amount of heat trapped inside the reactor between cycles, reducing the reactor stability, as observed by the narrower temperature plateau.[33] This is more important for monolithic RFR than for particulate RFR, because the lower bed porosity reduces the thermal inertia of the bed, being more prone the reactor to extinction.

Table 3. Summary of Operation Conditions in the Experiments Carried Out in the Monolithic Reverse-Flow Reactor

ID	Q_{G0} (m^3 s^{-1} (STP))	t_{sw} (s)	y_{G0} (ppm)
1	2.5×10^{-4}	100	1915
2	2.5×10^{-4}	100	4336
3	2.5×10^{-4}	200	1915
4	2.5×10^{-4}	200	4336
5	2.5×10^{-4}	200	4770
6	2.5×10^{-4}	300	940
7	2.5×10^{-4}	300	1915
8	2.5×10^{-4}	300	3614
9	2.5×10^{-4}	300	4336
10	2.5×10^{-4}	300	4770
11	2.5×10^{-4}	300	5240
12	2.5×10^{-4}	300	5421
13	2.5×10^{-4}	600	4336
14	2.5×10^{-4}	600	5421
15	2.5×10^{-4}	600	6324
16	2.5×10^{-4}	900	5421
17	5×10^{-4}	100	3975
18	5×10^{-4}	100	5421
19	5×10^{-4}	100	5782
20	5×10^{-4}	200	3975
21	5×10^{-4}	100	1915

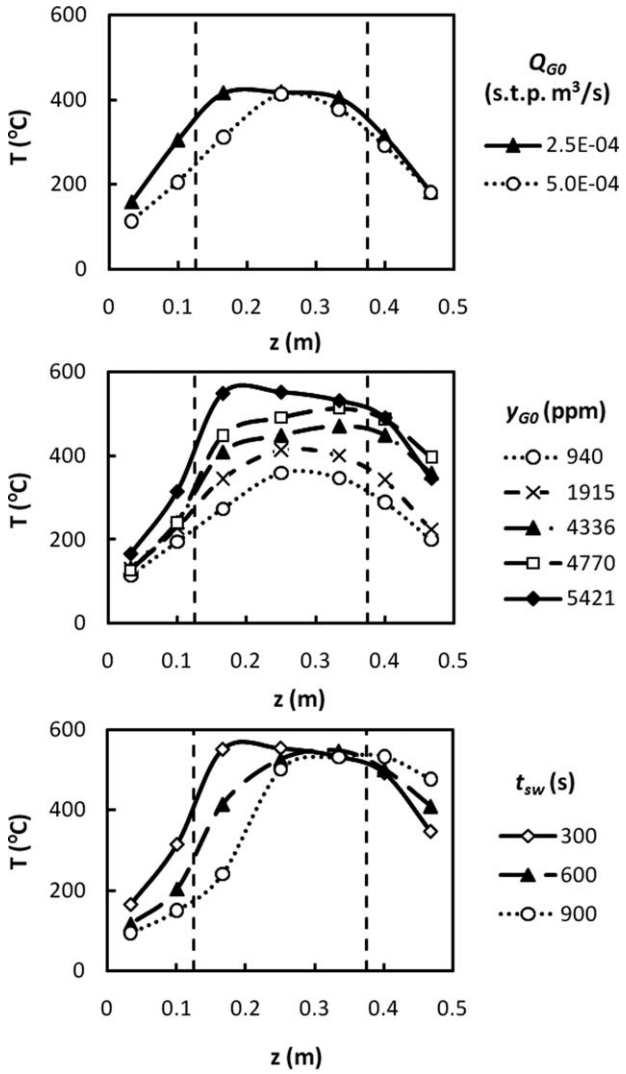

Figure 4. Influence of the main operating variables on reactor temperature profiles: experimental temperature profiles at the end of a half-cycle (gas flow from left to right).

(a) Total gas flow rate. $y_{G0} = 1915$ ppm. $t_{sw} = 100$ s. (b) Methane feed concentration. $t_{sw} = 300$ s. $Q_{G0} = 2.5 \times 10^{-4}$ m^3 s^{-1} (STP). (c) Switching time. $y_{G0} = 5421$ ppm. $Q_{G0} = 2.5 \times 10^{-4}$ m^3 s^{-1} (STP).

The feed concentration is an important operating variable, usually subjected to constant variations when treating typical industrial gaseous emissions.[34] In Figure 4b, the effect of this variable on the reactor performance has been studied in terms of the adiabatic temperature rise, maintaining constant the other two ($Q_{G0} = 2.5 \times 10^{-4}$ m^3 s^{-1} (STP) and $t_{sw} = 300$ s). The heat released by the reaction increases as the methane concentration in the feed increases, resulting in an increase of the width of the high temperature plateau and the value of the maximum temperature. This fact leads to higher reactor stability as reported previously in other works,[33] when working with particulate fixed-bed reactors. Moreover, if these results are compared with those reported in the literature at the same reaction conditions, but working with particulate RFR,[20] it is observed that the sensibility of the monolithic reactor to variations in inlet concentration is higher than the corresponding to particulate RFR.

Finally, the influence of the switching time is studied in Figure 4c. This variable regulates the amount of heat stored in the reactor between cycles, which can be very useful for monolithic RFR to avoid extinction. As a result, a strict control of the switching time must be imposed, so that reactor stability is maintained.[7,34,35] The experimental temperature profiles at the end of a half-cycle for three values of the switching time are shown in Figure 4c. For high switching times (900 s), the temperature plateau moves within a wider zone, resulting in a higher average outlet temperature, and thus more heat is expelled out of the reactor. As these experiments correspond to a high methane feed concentration ($y_{G0} = 5421$ ppm), the reactor is stable for a switching time value as high as 900 s, but in other situations with lower feed concentrations, smaller switching time values would be required, so that to maintain the reactor ignited.

Figure 4 has revealed that monolithic RFR exhibits a similar behavior as particulate RFR, but showing lower stability. This will be systematically analyzed in the last section of this work.

Validation of the Mathematical Model

The 1D heterogeneous mathematical model presented before has been validated with experimental data from the bench-scale monolith RFR, described in the Experimental device section. As the bench-scale reactor operates under adiabatic conditions, the validated model can be used to simulate industrial RFR (with large diameter, and hence an intrinsic adiabatic behavior).

Simulations from the mathematical model have been carried out for comparison purposes for all the experiments. In all the cases, the reactor inlet is fed at room temperature ($T_{G0} = 25°C$, $p_0 = 1.01$ bar), and the reactor bed is initially preheated up to 400°C. Table 3 lists the operating conditions that have been varied in the experiments. Physical properties of the catalytic beds and kinetic parameters are summarized in Tables 1 and 2, respectively. As a general trend, good correspondence between experiments and simulations has been found. Temperature evolution plots allow comparing experimental results and simulations, as shown in Figure 5 for two different experiments (one for a switching time of 100 s, left column, and the other for 300 s, right column). Total gas flow rate and methane feed concentration have been kept constant during the experiment to 2.5×10^{-4} m^3 s^{-1} (STP) and 1915 ppm, respectively. The simulated evolution of the temperature practically matches the experimental one. The most important discrepancies are detected in the inert bed ($z = 0.100$ m) and during cooling half-cycles. This is explained because of the difficulty to get perfect adiabatic conditions with the proposed temperature control system device when high cooling rates are demanded. As this only happens at the ends of the reactor bed, where temperature changes more drastically and the deviation from adiabatic conditions is small, the center of the reactor is not affected.

The performance of the mathematical model can also be illustrated using temperature profiles plots, as observed in Figure 6, where the simulated temperature profiles (lines) have been compared to the experimental ones (symbols) at

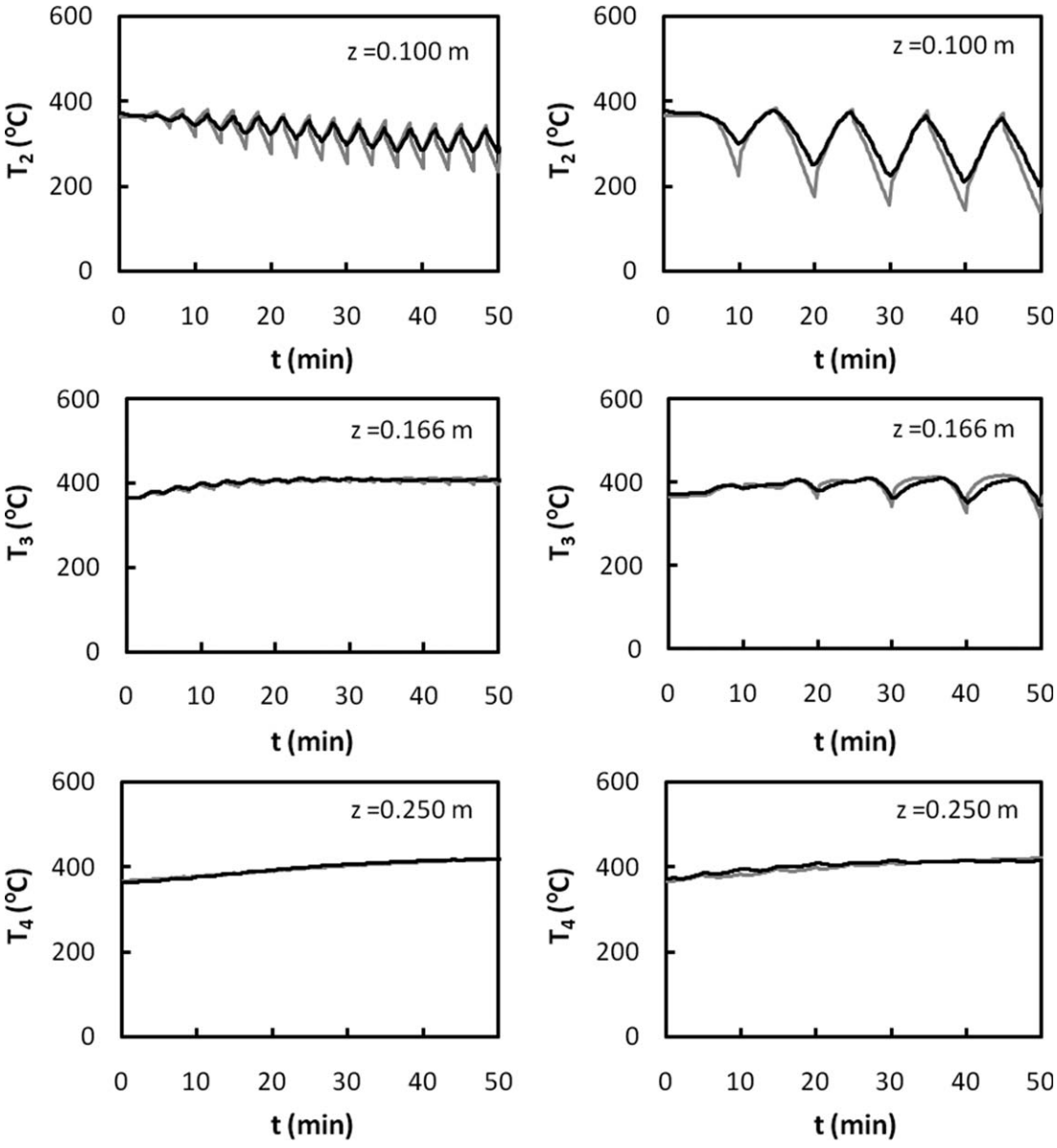

Figure 5. Validation of the RFR mathematical model: evolution of the temperature measured at different points of the bed with operation time.

$Q_{G0} = 2.5 \times 10^{-4}$ m^3 s^{-1} (STP). $y_{G0} = 1915$ ppm methane. Left column: $t_{sw} = 100$ s. Right column: $t_{sw} = 300$ s. (▬) Experiments, (▬) simulations.

the beginning, the middle, and the end of a direct half-cycle (with gas flowing from left to right). This way, the reactor performance is compared at different times during a sole half-cycle. In this case, total gas flow rate is 2.5×10^{-4} m^3 s^{-1} (STP), methane inlet concentration is 4336 ppm, and also two switching time values have considered (200, left graph, and 600 s, right graph). The other variables, geometric and physical properties are the same as for the experiments of Figure 5. In these experiments, the heat released by the reaction has been doubled with respect to the experiments of Figure 5, resulting in a different reactor performance. Anyway, the correspondence observed between experiments and simulations is also good, being the most important discrepancies focused on the reactor ends and during the cooling stage, as explained before. These discrepancies are more important on increasing the switching time, because the high temperature plateau is allowed to move wider, so the cooling shortage of the temperature control system affects to a larger part of the reactor bed. This means that this bench-scale RFR is only suitable for working under near-adiabatic conditions at not very high switching time values. Consequently, only the experiments with switching times values lower or equal than 600 s have been considered for model validation.

In conclusion, the mathematical model proposed to simulate the behavior of RFR, using monoliths as both inert and catalyst beds, has been successfully validated with experimental data from a bench-scale device for the catalytic

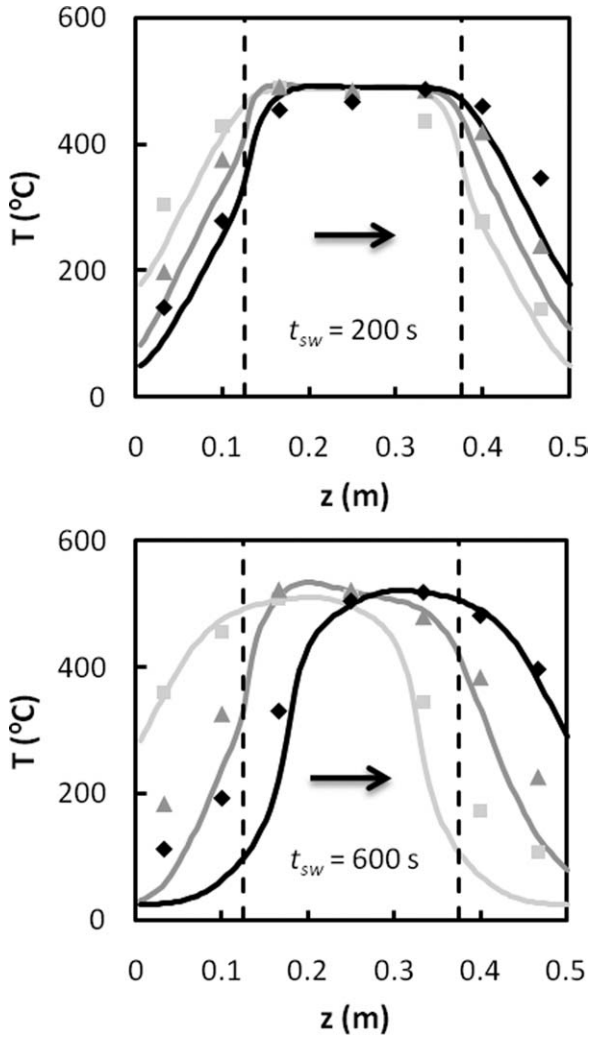

Figure 6. Validation of the RFR mathematical model: temperature profiles for one half-cycle starting at 3600 s.

Symbols: experiments; lines: simulations. Beginning (▬), middle (▬), and end (▬) of the cycle. Flow direction is indicated by the arrow. $Q_{G0} = 2.5 \times 10^{-4}$ m^3 s^{-1} (STP). $y_{G0} = 4336$ ppm methane.

combustion of methane. Hence, this model can be considered validated and valid for the simulation of the RFR behavior and the design of industrial-scale reactors.[32]

Comparison Between Particulate and Monolith RFR

The model validated in the previous section has been used to compare the performance of large-scale RFR using both particulate and monolith beds. Particulate beds have been simulated according to models validated in the previous works.[10,20,34–36]

Particulate and monolithic beds exhibit different physical and transport properties, resulting in a difficult comparison. For this reason and to carry out a systematic comparison, both bed types have been compared using the so-called design curves. These curves consist of a plot of the pseudo-steady-state outlet conversion against reactor length (Figures 7 and 8). It must be taken into account that one single computer simulation of the RFR model up to the pseudo-steady state (50 cycles have been found to be enough to achieve the pseudo-steady state) will produce only one point of the design curve. Subsequent simulations for different reactor lengths are necessary to obtain the entire curve. On the contrary, one simulation of a fixed-bed reactor with unidirectional flow will directly produce the entire reactor design curve. As shown, RFR design curves delimit two zones separated by a sharp step in conversion. Below a characteristic reactor length value, stable operation of the reactor is not possible, whereas above this value near complete conversion is reached. This characteristic reactor length value can be used to compare the performance of particulate and monolithic beds. Design curves can be easily used to design a RFR by simply selecting the desire outlet conversion and determining the required reactor length from the curve.

Different operation conditions may result in differences in reactor performance for particulate and monolith RFR. For this reason, design curves have been constructed for different surface gas velocities and methane inlet concentrations. As explained in previous sections, these two variables are within the most important parameters affecting the RFR behavior. The rest of physical properties and operating conditions are summarized in Tables 2 and 4. The switching time has been considered constant for all the simulations, though affecting the RFR behavior, because it is typically selected based on the expected lifetime of the switching valves (in general, the

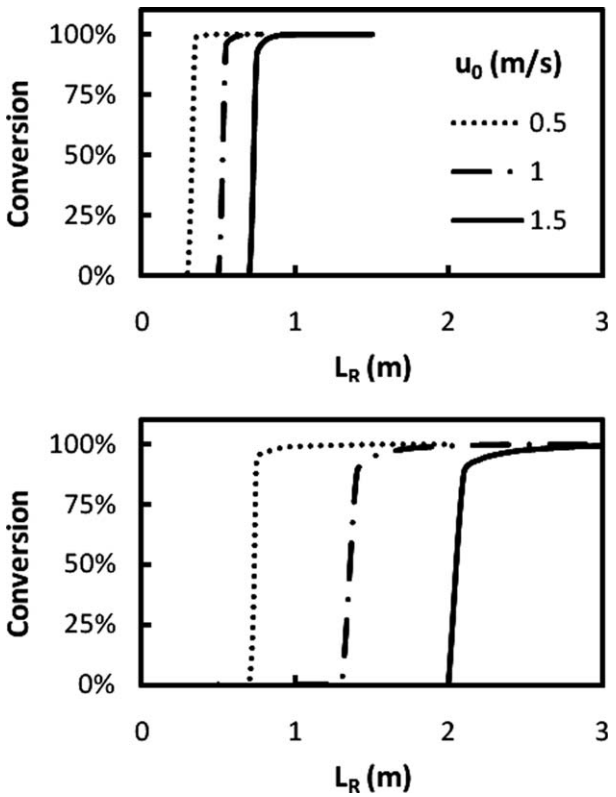

Figure 7. Design curves for different surface velocities for methane combustion in the particulate (upper graph) and monolithic (lower graph) beds.

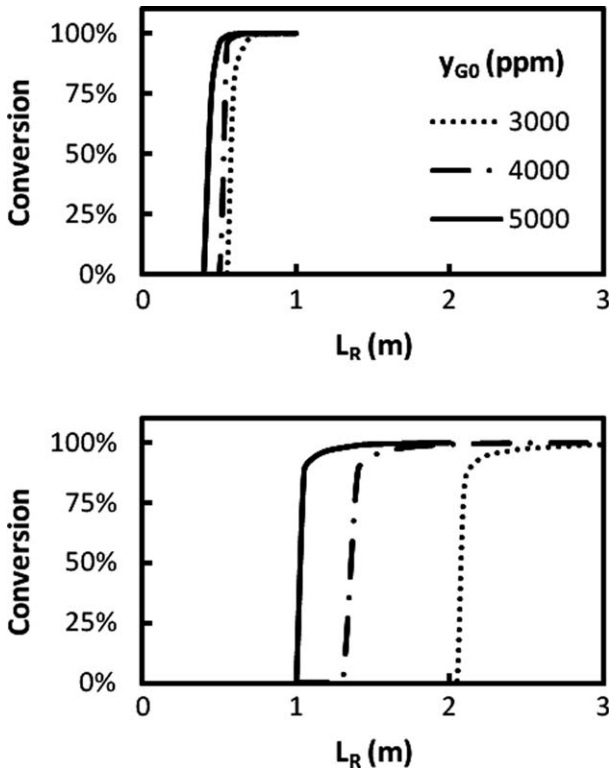

Figure 8. Design curves for different methane feed concentrations for the combustion of methane in the particulate (upper graph) and monolithic (lower graph) beds.

valves cab give up to 500,000 strokes). Thus, if a low switching time is selected, the designed reactor length will be lower, but also the lifetime of the valves. The value of 300 s selected in this study represents a good compromise, corresponding to a valve lifetime of about 4.75 years of continuous operation.[7,32] It should be noted that catalyst activity per unit of catalyst mass is the same for both bed types, corresponding to the same catalyst but with different shapes.

Figure 7 shows the influence of surface velocity. This variable determines not only the amount of hydrocarbon to be treated but also the velocity of the moving temperature plateau. For this reason, on increasing the surface velocity, a marked increase in the reactor length necessary to achieve stable operation is also observed. When comparing particulate (upper graph) and monolithic beds (lower graph), it is found that the second one requires a larger reactor length to achieve similar outlet conversions, for all the surface velocity values considered. This is explained by the difference in volumetric heat capacity ($(1-\varepsilon)\rho_S C_{pS}$) between beds. Thus, the lower bed porosity of the monolithic bed (Table 4) reduces the thermal inertia of the system, resulting in a higher speed of the high temperature plateau. As the switching time is the same for both bed types ($t_{sw} = 300$ s), the monolithic bed requires a higher reactor length to trap the heat of reaction between cycles, and thus obtain stable operation. Similar behavior is described in the literature for other unsteady-state devices, such as recuperative catalytic combustors.[37]

The influence of the inlet concentration of methane is studied in Figure 8. On increasing methane feed concentration, the heat released by the reaction also increases, resulting in a reduction of the necessary reactor length to achieve stable operation. The differences between particulate (upper graph) and monolithic (lower graph) beds are remarkable. As shown in Figure 8, in comparison with the particulate bed, the monolith bed is highly affected by inlet concentration, for example, increasing the concentration from 3000 to 5000 ppm results in a decrease of the stable reactor length from 2 to 1 m. This is very important to design a suitable control system for the RFR, which is one of the drawbacks of this

Table 4. Bed Properties Used in the Comparison of Particulate and Monolith Beds

Simulation Parameters	
Inlet gas temperature, T_{G0} (°C)	25
Inlet pressure, p_0 (bar)	1.01
Switching time, t_{sw} (s)	300
Preheating bed temperature, T_{ph} (°C)	400
Catalytic bed fraction	50%
Bed porosity, ε (particulate/monolith)	0.4/0.6
Particle diameter/hydraulic diameter (m)	$5 \times 10^{-3}/1.2 \times 10^{-3}$
Solid density, ρ_S (kg m^{-3})	2000
Solid heat capacity, C_{pS} (J kg^{-1} K^{-1})	900
Solid thermal conductivity, k_S (W m^{-1} K^{-1})	1

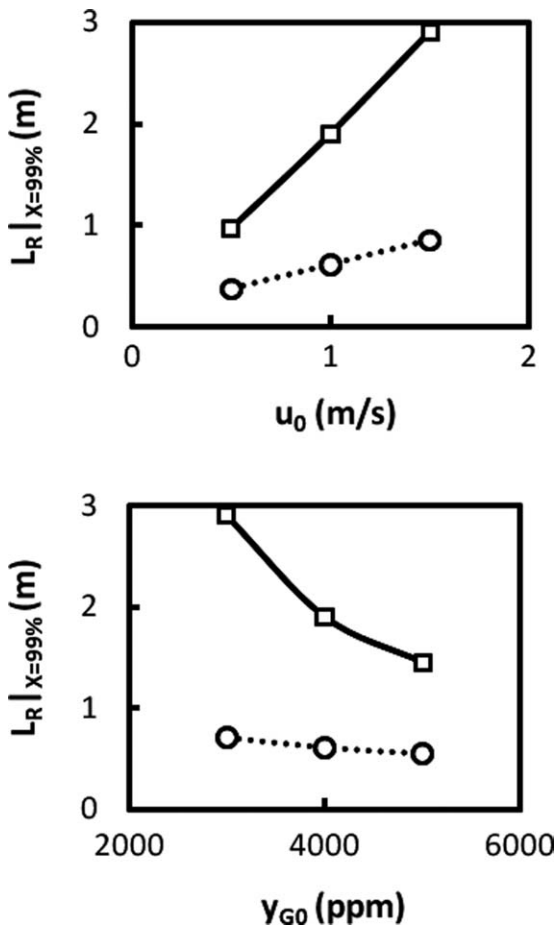

Figure 9. RFR designs corresponding to 99% conversion for particulate (•••) and monolith (▬) beds as a function of gas surface velocity and methane feed concentration.

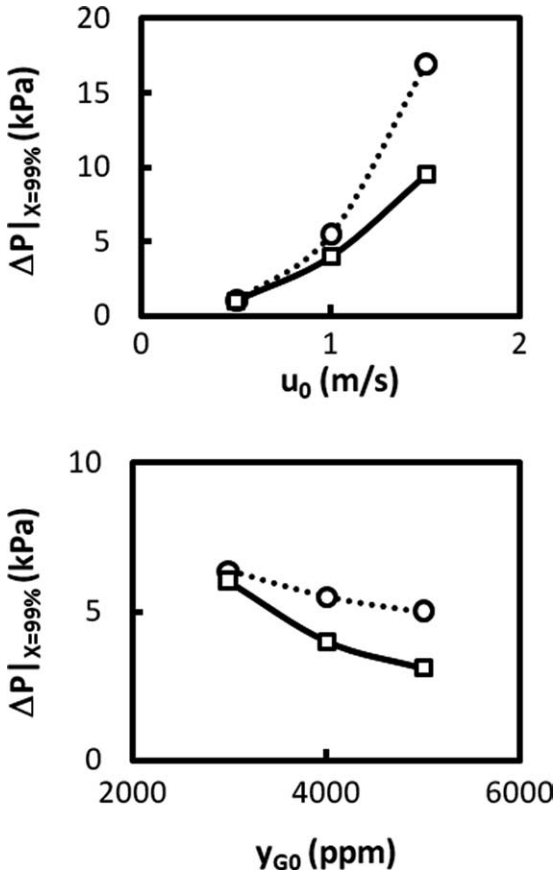

Figure 10. Pressure drop per unit of length for the designs of Figure 9 for particulate (•••) and monolith (▬) beds as a function of gas surface velocity and methane feed concentration.

technology. At this point, there are authors who propose control strategies based on changes of the switching time or forced increases of the hydrocarbon concentration.[7,35] This second approach seems to be appropriate for working with monolithic RFR, as it is observed that the monolithic reactor is more sensitive to variations on inlet concentration.

Design curves can also be used to design the RFR. Thus, for a desired outlet conversion of 99%, the required reactor length is read from the curve. In Figure 9, the different reactor designs are compared as a function of the two operation variables selected: surface velocity and methane inlet concentration. As shown, monolithic RFR always exhibits the higher reactor lengths, resulting in a more unstable reactor bed. It should be noted that 99% reactor length depends linearly on surface velocity for RFR. In general, similar conclusions are obtained for fixed-bed reactors with unidirectional flow. Nevertheless, the slope of the line is higher for the case of the monolithic bed, resulting in a higher influence of surface velocity for this type of bed. Similar conclusions can be obtained for methane inlet concentration, but in this case, as explained before, the influence on the design is on the other direction, resulting in a negative slope.

The pressure drops of the designs shown in Figure 9 are depicted in Figure 10. It should be noted that although pressure drop of monolithic reactors is lower, designs shown in Figure 9 are done with higher reactor lengths of the monolithic reactor. In all the simulations, the reactor pressure drop of the monolithic bed has been found to be lower. The influence of the operating variables is explained as follows. An increase in surface velocity causes a direct increase in pressure drop, but this increase is more pronounced for the particulate bed. Similar findings are obtained for the inlet concentration, but in the opposite direction: higher concentrations results in lower pressure drops. This is mainly explained by the lower reactor length required at higher concentrations.

Summarizing, despite requiring higher reactor lengths, monolithic beds offer lower reactor pressure drops than particulate beds, for the same operating conditions (surface velocity, inlet concentration, outlet conversion, switching time, etc.). However, the discrepancies for the case of low surface velocity and low inlet concentration are very short, so in these situations the advantages of monolithic RFR are not clear. The final decision should be based on the economical balance of both bed types. In the economical balance, only costs being affected by the bed type are considered.[32] Thus, total reactor cost can be split in investment costs, mainly catalyst costs, and annual costs, mainly compression costs; the first one is proportional to the reactor length, calculated using Figure 9, while the second one is proportional to the pressure drop, in Figure 10. As shown, Figures 9 and 10, and other similar figures constructed for another operating conditions or physical properties, are needed to decide the best design.

Conclusions

The influence of the main operating variables (total gas flow rate, inlet concentration, and switching time) on the reactor performance has been experimentally studied in this work. The main handicap in the application of monolithic catalysts to RFR technology is their lower thermal inertia. Thus, high gas flow rates, low inlet concentration, and high switching time values reduce the heat trapped inside the reactor between cycles, being the reactor more prone to extinction.

A heterogeneous 1D dynamic model for adiabatic reverse-flow monolithic reactors is validated by comparison of the simulations with more than 20 experiments from the bench-scale device; simulations accurately predicting the experiments. Once the model was validated, a systematic comparison by simulations between particulate and monolithic RFR has been carried out. As the use of monolith catalysts is necessary for dealing with high flow rates, it is proposed in this work to compensate its lower stability by increasing the reactor lengths, design rules being suggested in the manuscript.

Acknowledgments

This work was financed by a Research Project of the Regional Plan for Research, Development and Innovation of the Regional Asturian Government (Spain) (IB05-103).

Notation

a_G = $(4/D_h)$, surface-gas volume ratio, m^{-1}
a_S = $(4/D_h)(\varepsilon/(1-\varepsilon))$, surface-solid volume ratio, m^{-1}
b = reaction exponent
Ca = Carberry number

C_G = total molar concentration of the gas phase, mol m^{-3}
C_P = heat capacity, J kg^{-1} K^{-1}
D_{AB} = methane–air molecular diffusion coefficient, m^2 s^{-1}
D_{ax} = axial dispersion coefficient, m^2 s^{-1}
D_{eff} = $(\varepsilon_{pore}/\tau_{pore})(1/D_{AB} + 1/D_K)^{-1}$, effective diffusion coefficient in the porous washcoat layer, m^2 s^{-1}
D_K = Knudsen diffusion coefficient, m^2 s^{-1}
D_h = hydraulic diameter, m
$\langle d_{pore} \rangle$ = mean pore diameter, m
E_a = activation energy, J mol^{-1}
f_F = 24/*Re*, Fanning friction factor
f_w = washcoat volume fraction
F_{tot} = total gas flow rate, mol s^{-1}
h = gas–solid heat transfer coefficient, W m^{-2} K^{-1}
k_m = kinetic constant, mol kg^{-1} s^{-1} Pa^{-b}
k_m^0 = preexponential factor, mol kg^{-1} s^{-1} Pa^{-b}
k_G = gas–solid mass transfer coefficient, m s^{-1}
L = length, m
L_w = washcoating thickness, m
M_{cat} = catalyst mass, kg
Nu = Nusselt number
p = pressure, Pa
Pr = Prandtl number
Q_{G0} = feed total gas flow rate, $m^2 s^{-1}$
$(r_j)_m$ = reaction rate, mol kg^{-1} s^{-1}
R = ideal gas constant, J mol^{-1} K^{-1}
Re = Reynolds number
Sc = Schmidt number
Sh = Sherwood number
t = time, s
t_{sw} = switching time, s
T = temperature, K
u = surface velocity, m s^{-1}
v = linear gas velocity, m s^{-1}
X = conversion
y = molar fraction
z = axial coordinate, m

Greek letters

ΔH = heat of reaction, J mol^{-1}
ΔT_{ad} = adiabatic temperature rise, °C
ε = porosity
ϕ = Thiele modulus
κ = thermal conductivity
η = internal effectiveness factor
ρ = density
τ = tortuosity

Subscripts

0 = feed conditions
ax = axial
cat = catalyst
exp = experimental
G = gas
j = j-component
max = maximum
ph = preheating
pore = porous washcoat layer
R = reactor
S = solid
tot = total

Literature Cited

1. Manahan SE. *Environmental Chemistry*. Boca Ratón, FL: CRC-Press, 2000; *Chapter 14*.
2. Hurtado P, Ordóñez S, Sastre H, Díez FV. Combustion of methane over palladium catalysts in presence of inorganic compounds: inhibition and deactivation phenomena. *Appl Catal B*. 2004;47:85–93.
3. Su S, Agnew J. Catalytic combustion of coal mine ventilation air methane. *Fuel*. 2006;85:1201–1210.
4. Marín P, Ordóñez S, Díez FV. Procedures for heat recovery in the catalytic combustion of lean methane-air mixtures in a reverse flow reactor. *Chem Eng J*. 2009;147:356–365.
5. Matros YS, Bunimovich GA. Reverse-flow operation in fixed bed catalytic reactors. *Catal Rev Sci Eng*. 1996;38:1–68.
6. Budzianowski WM, Miller R. Superadiabatic lean catalytic combustion in a high pressure reactor. *Int J Chem React Eng*. 2009;7:A20.
7. Barresi AA, Baldi G, Fissore D. Forced unsteady-state reactors as efficient devices for integrated processes: case histories and new perspectives. *Ind Eng Chem Res*. 2007;46:8693–8700.
8. Kolios G, Frauhammer J, Eigenberger G. Autothermal fixed-bed reactor concepts. *Chem Eng Sci*. 2000;55:5945–5967.
9. Eigenberger G, Kolios G, Nieken U. Thermal pattern formation and process intensification in chemical reaction engineering. *Chem Eng Sci*. 2007;62:4825–4841.
10. Fissore D, Barresi AA, Baldi G, Hevia MAG, Ordóñez S, Díez FV. Design and testing of small-scale unsteady-state afterburners and reactors. *AIChE J*. 2005;51:1654–1664.
11. Vandebeld L, Westerterp KR. Air purification in a reverse-flow reactor: model simulations vs. experiments. *AIChE J*. 1996;42:1139–1148.
12. Heck RM, Gulati S, Farrauto RJ. The application of monoliths for gas phase catalytic reactions. *Chem Eng J*. 2001;82:149–156.
13. Nieken U, Kolios G, Eigenberger GA. Fixed-bed reactors with periodic flow reversal: experimental results for catalytic combustion. *Catal Today*. 1994;20:335–350.
14. Eigenberger G, Nieken U. Catalytic cleaning of polluted air: reaction engineering problems and new solutions. *Int Chem Eng*. 1994; 31:4–16.
15. Ramdani K, Pontier R, Schweich D. Reverse flow reactor at short switching periods for VOC combustion. *Chem Eng Sci*. 2001;56:1531–1539.
16. Litto R, Hayes RE, Sapoundjiev H, Fuxman A, Forbes F, Liu B, Bertrand F. Optimization of a flow reversal reactor for the catalytic combustion of lean methane mixtures. *Catal Today*. 2006;117:536–542.
17. Gosiewski K, Matros YS, Warmuzinski K, Jaschik M, Tanczyk M. Homogeneous vs. catalytic combustion of lean methane-air mixtures in reverse-flow reactors. *Chem Eng Sci*. 2008;63:5010–5019.
18. Marín P, Hevia MAG, Ordóñez S, Díez FV. Combustion of methane lean mixtures in reverse flow reactors: comparison between packed and structured catalyst beds. *Catal Today*. 2005;105:701–708.
19. Hevia MAG, Ordóñez S, Díez FV. Effect of wall properties on the behaviour of bench-scale reverse flow reactors. *AIChE J*. 2006;52:3203–3209.
20. Hevia MAG, Ordóñez S, Díez FV. Effect of the catalyst properties on the performance of reverse flow reactor for methane combustion in lean mixtures. *Chem Eng J*. 2007;129:1–11.
21. Escandón LS, Ordóñez S, Vega A, Díez FV. Oxidation of methane over palladium catalysts: effect of the support. *Chemosphere*. 2005;58:9–17.
22. Liu B, Hayes RE, Yi Y, Mmbaga J, Checkel MD, Zheng M. Three dimensional modelling of methane ignition in a reverse flow catalytic converter. *Comput Chem Eng*. 2007;31:292–306.
23. Fissore D, Barresi AA. On the influence of the catalyst physical properties on the stability of forced unsteady-state after-burners. *Chem Eng Res Des Trans IChemE A*. 2003;81:611–617.
24. Hayes RE, Kolaczkowski ST. *Introduction to Catalytic Combustion*. Amsterdam: Gordon and Breach Science Publishers, 1997.
25. Ullah U, Waldram SP. Monolithic reactors: mass transfer measurements under reacting conditions. *Chem Eng Sci*. 1992;47:2413–2418.
26. Hayes RE, Kolaczkowski ST, Li PKC, Awdry S. The palladium catalysed oxidation of methane: reaction kinetics and the effect of diffusion barriers. *Chem Eng Sci*. 2001;56:4815–4835.
27. Hurtado P, Ordóñez S, Sastre H, Díez FV. Development of a kinetic model for the oxidation of methane over Pd/Al_2O_3 at dry and wet conditions. *Appl Catal B*. 2004;51:229–238.
28. Berger RJ, Kapteijn F, Moulijn JA, Marin GB, De Wilde J, Olea M, Chen D, Holmen A, Lietti L, Tronconi E, Schuurman Y. Dynamic methods for catalytic kinetics. *Appl Catal A*. 2008;342:3–28.
29. Gosiewski K, Warmuzinski K. Effect of the mode of heat withdrawal on the asymmetry of temperature profiles in reverse-flow reactors. Catalytic combustion of methane as a test case. *Chem Eng Sci*. 2007;62:2679–2689.
30. Petersen EE. A general criterion for diffusion influenced chemical reactions in porous solids. *Chem Eng Sci*. 1965;20:587.

31. Matros YS, Bunimovich GA. Control of volatile organic compounds by the catalytic reverse process. *Ind Eng Chem Res*. 1995;34:1630–1640.
32. Marín P, Ordóñez S, Díez FV. Simplified design methods of reverse flow catalytic combustors for the treatment of lean hydrocarbon-air mixtures. *Chem Eng Process*. 2009;48:229–238.
33. van de Beld B, Borman RA, Derkx OR, van Woezik BAA, Westerterp KR. Removal of volatile organic compounds from polluted air in a reverse flow reactor: an experimental study. *Ind Eng Chem Res*. 1994;33:2946–2956.
34. Hevia MAG, Ordóñez S, Díez FV, Fissore D, Barresi AA. Design and testing of a control system for reverse-flow catalytic afterburners. *AIChE J*. 2005;51:3020–3027.
35. Marín P, Ho W, Ordóñez S, Díez FV. Demonstration of a control system for combustion of lean hydrocarbon emissions in a reverse flow reactor. *Chem Eng Sci*. 2010;65:54–59.
36. Marin P, Ordóñez S, Díez FV. Combustion of toluene-hexane binary mixtures in a reverse flow catalytic reactor. *Chem Eng Sci*. 2008;63:5003–5009.
37. Budzianowski WM, Miller R. Design of dynamics of a recuperative catalytic combustor: enhancement in operation and control. *Chem Prod Process Model*. 2009;4:A11.

Manuscript received Nov. 27, 2009, and revision received Feb. 2, 2010.